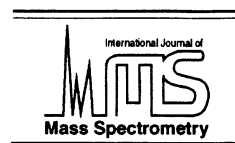




ELSEVIER

International Journal of Mass Spectrometry 192 (1999) 267–280



# Spontaneous and induced dissociation of singly and multiply charged fullerene ions

F. Biasioli, T. Fiegele, C. Mair, G. Senn, S. Matt, R. David, M. Sonderegger, A. Stamatovic<sup>1</sup>, P. Scheier, T.D. Märk\*

*Institut für Ionenphysik, Leopold Franzens Universität, Technikerstrasse 25, A-6020 Innsbruck, Austria*

Received 12 January 1999; accepted 9 March 1999

## Abstract

Using newly developed experimental techniques we have studied spontaneous (metastable) dissociation, electron-induced dissociation, and surface-induced dissociation reactions of singly and multiply charged fullerene ions. In particular, we will discuss results concerning (1) competition in spontaneous decay reactions between evaporation of neutral and ionized fragments, thereby extending our own previous studies on the spontaneous decay of multiply charged fullerene ions, (2) electron induced dissociation for singly and doubly charged  $C_{60}$  ions with special emphasis on the time dependence of kinetic energy release distribution thereby extending the recent cross section measurements of Salzborn and co-workers [Phys. Rev. Lett. 71 (1993) 3439], and (3) surface induced dissociation of singly and doubly charged  $C_{58}^{z+}$  ions thereby extending previous studies by Kappes and co-workers [J. Chem. Phys. 104 (1996) 3629, 3638] on singly charged  $C_{60}$  ions. (Int J Mass Spectrom 192 (1999) 267–280) © 1999 Elsevier Science B.V.

*Keywords:* Fullerene ions; Spontaneous decay; Electron-induced dissociation; Surface-induced processes; Multiply charged ions

## 1. Introduction

Strongly bound, highly excited finite atomic systems will relax by either emitting electrons, neutral particles, or a continuous spectrum of photons. These reactions are the molecular analogues to thermionic emission, evaporation, and black body radiation in solid state physics. Moreover, multiply charged systems may decay via fission reactions ejecting charged

rather than neutral fragments analogous to nuclear fission. Coulomb repulsion within a multiply charged molecule or cluster leads to the destruction of the ion if the corresponding binding energies are weaker than the effective Coulomb force [1]. Because of their special structure, fullerenes [2] are known to show exceptional stability against these charge separation fragmentation processes [3–10] thus allowing the production and observation of multiply charged  $C_{60}$  ions [7,8,11].

The energetics and dynamics of dissociation reactions of neutral and charged fullerenes have received considerable attention over the past decade [12–24]. Methods used to study these fragmentation reactions include the following.

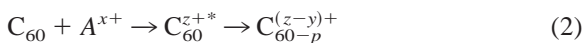
\* Corresponding author. Adjunct professor at Dept. Plasma-physics, Comenius University, Mlynska Dolina F2, 84215 Bratislava, Slovakia.

<sup>1</sup> Permanent address: Faculty of Physics, P.O. Box 638, Yu-11001 Beograd, Yugoslavia.

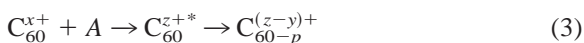
Electron and photon induced dissociative ionization



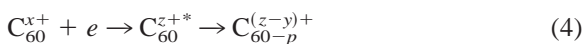
Charge transfer dissociative ionization



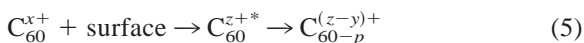
Collision-induced dissociation



Electron-induced dissociation



Surface-induced dissociation



Here we will summarize recent results obtained in our laboratory using newly developed experimental techniques to study spontaneous (metastable), electron-induced and surface-induced dissociations of singly and multiply charged fullerenes. In particular we will discuss (1) competition in spontaneous decay reaction (1) with  $y = 0$  and 1 thereby extending our own previous studies on the spontaneous decay of multiply charged fullerene ions [25–28], (2) electron induced dissociation for singly and doubly charged  $\text{C}_{60}$  ions thereby extending the cross section measurements of Salzborn and co-workers [29] and our own preliminary study on the kinetic energy release [30], and (3) surface-induced dissociation of singly and doubly charged  $\text{C}_{58}$  ions thereby extending previous studies by Kappes and co-workers on singly charged  $\text{C}_{60}$  ions [31,32].

## 2. Experimental

Details of the main components of the experimental setup used in the present work to study metastable and electron-induced decay reactions have been described previously [26,33]. As shown in Fig. 1, the apparatus used consists of a modified Nier type electron impact ion source, a fullerene molecular beam source and a high resolution double focusing

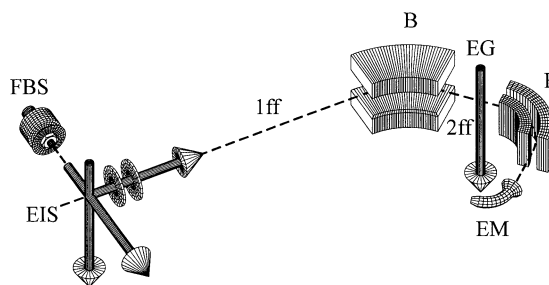


Fig. 1. Schematic view of two sector field mass spectrometer system used to study electron-induced and metastable decay reactions in the second field-free region. FBS: fullerene beam source, EIS: electron impact ion source, B: magnetic sector field, E: electric sector field, EG: electron gun, EM: electron multiplier, 1ff: first field-free region, 2ff: second field-free region.

two-sector field mass spectrometer (reversed geometry) with a mass range of 10 000 amu at a nominal acceleration voltage  $U$  of 3 kV. The pure fullerene sample is evaporated in a temperature controlled Knudsen type oven typically operated at around 950 K. After entering the ion source via a skimmer and a collimator the effusive molecular beam is crossed at right angles by an electron beam of variable energy and current. Alternatively, test molecules to be ionized can be introduced into the collision chamber of the ion source via a conventional capillary leak gas inlet system (not shown in Fig. 1).

The resulting ions are then extracted from the ion source by a weak electric field and accelerated to a translational energy of  $3z$  keV, with  $z$  the charge of the ions. After passing through a first field-free region (1ff for short, length 61 cm), the ions are momentum analyzed by a  $48.5^\circ$  magnetic sector before entering a second field-free region (2ff, length 33.3 cm). Next the ions are energy analyzed by a  $90^\circ$  electric sector and detected by an electron multiplier operated in the single-ion counting mode.

Unimolecular dissociations occurring in the two field-free regions of this double focusing mass spectrometer can be identified by decoupling the two analyzing fields [34]. In order to study here the metastable or electron-induced decay of a mass selected fullerene ion, we are first selecting a specific ion with the magnetic sector field and then analyzing decay reactions in the 2ff by varying the voltage of the

electric sector field (MIKE scan technique [34]). The positions of the peaks obtained in such a MIKE (mass analysed ion kinetic energy) spectrum (Fig. 2 shows as an example a corresponding spectrum for electron-induced ionization and dissociative ionization of mass selected  $C_{60}^{2+}$ ) can be directly related to the mass-to-charge ratio of the product ions thus allowing a definitive identification of the reaction products. A simple equation relates the value  $E^*$  at the center of the MIKE peak to the sector field voltage of the precursor ion  $E$  and the mass per charge ratios of the precursor ion and daughter ion,  $m_1/z_1$  and  $m_2/z_2$ , respectively, by

$$E^* = E(m_2z_1/m_1z_2) \quad (6)$$

Furthermore, it is possible to deduce from the shape of these MIKE peaks the kinetic energy release distribution (KERD) of the fragment ions by taking the first derivative of the measured MIKE peak and by using the relationship

$$\text{KER} = \frac{m_1^2z_2^2eU}{16m_2m_3z_1} \left( \frac{\Delta E^*}{E} \right)^2 \quad (7)$$

to relate the measured  $\Delta E^*$  (which is the width of the metastable peak) to the total kinetic energy released in the decay reaction. Moreover, by taking the first moment of this KERD also the mean kinetic energy release  $\langle \text{KER} \rangle$  of the corresponding decay reaction can be derived, for more details see also earlier studies from our laboratory involving this method [27,28,35,36].

As mentioned previously, in the present work we have not only analyzed the spontaneous (metastable) decay of fullerenes, but a second goal was to investigate the electron-induced fragmentation of mass selected fullerene ions. For this purpose we have recently developed a high-performance electron gun [37,38], which has been mounted in the 2ff approximately halfway between the magnetic and the electric sector fields. Thus it is possible to cross the ion beam perpendicularly with a collimated electron beam of up to 15 mA. In contrast to previous studies on this subject in our laboratory with a much simpler electron gun [30] we have been able to improve here the

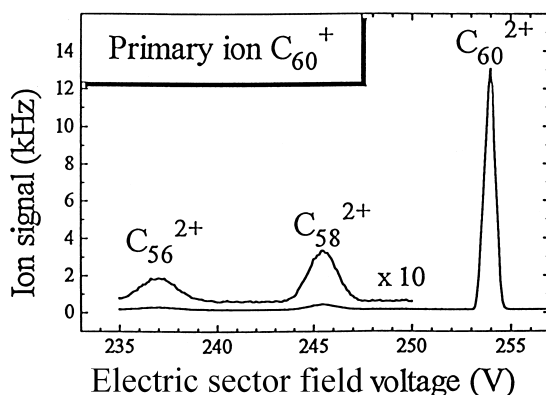


Fig. 2. MIKE spectrum showing the doubly charged parent and two fragment ions produced by electron impact ionization and dissociative ionization (using 250 eV electrons) of mass selected  $C_{60}^{2+}$ . This spectrum has been recorded with a 2 mm beta slit and a wide open mass spectrometer exit slit.

product ion count rate by a factor of about 100. As an example Fig. 2 gives a section of the electron-induced MIKE spectrum produced by electron impact of mass selected  $C_{60}^{2+}$  ions showing doubly charged parent and two doubly charged fragment ions produced via ionization and dissociative ionization reactions, respectively. It is interesting to note that the major ion exhibits count rates of more than 10 kHz at background rates of less than 0.01 kHz.

Finally, we are presenting in Fig. 3 the tandem mass spectrometer system BESTOF recently constructed for the study of ion–surface collisions [39]. It consists of a Nier-type ion source, a first mass spectrometer (double focusing two-sector field mass spectrometer), a collision chamber and a second mass spectrometer (time of flight mass spectrometer). The neutral  $C_{60}$  beam is again produced by evaporating pure  $C_{60}$  powder in a temperature-controlled Knudsen type oven. The  $C_{60}$  beam enters transversely into a Nier-type electron impact ion source. Furthermore, a direct gas inlet may be substituted for the fullerene source for the investigation of conventional ion surface collisions. Neutral molecules or fullerenes are ionized by impacting them with electrons whose energy can be varied from below the ionization energy up to about 500 eV.

The ions produced are extracted from the ion

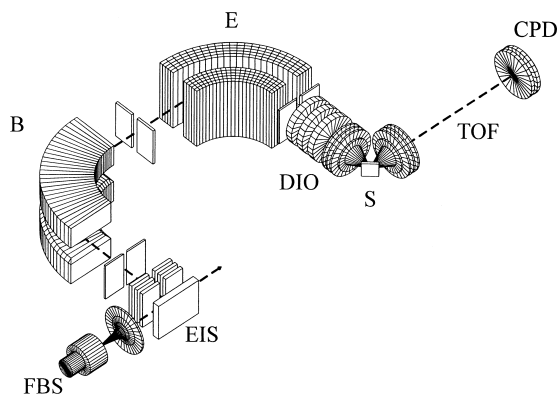


Fig. 3. Schematic view of the tandem mass spectrometer BESTOF consisting of an ion source, a two sector field mass spectrometer, a collision region, and a time of flight mass spectrometer. FBS: fullerene beam source, EIS: electron impact ion source, B: magnetic sector field, E: electric sector field, DIO: deceleration ion optics, S: surface, TOF: time of flight mass spectrometer, CPD: channel plate detector.

source region and accelerated to about 3 keV for mass and energy analysis by the double-focusing two-sector field mass spectrometer. The nominal mass resolution of this two-sector field mass spectrometer exceeds at 3 keV a value of 10 000 and thus easily allows the selection of isotopically pure primary ions. After passing the exit slit of the mass spectrometer, ions are refocused by an Einzel lens and the deceleration optics positioned in front of the stainless steel surface. Shielding the surface with conical shield plates minimizes field penetration effects. The incident impact angle  $\delta$  of the primary ions at the surface (about  $45^\circ$ ) is chosen to maximize the signal and the scattering angle is fixed at  $90^\circ$  (for a variation of the scattering angle and its influence on the secondary ion yields see [40]). In the present studies, experiments have been carried out using a stainless steel surface under ultrahigh vacuum conditions ( $10^{-10}$  Torr) maintained in our bakeable turbopumped collision chamber. However, even these conditions do not exclude the production of monolayers of hydrocarbon contaminants (pump oil, etc.) on the surface whenever the valve between the mass spectrometers and the surface collision chamber is opened and the pressure in the target region is rising to the  $10^{-9}$  Torr range.

The collision energy of ions impacting on the

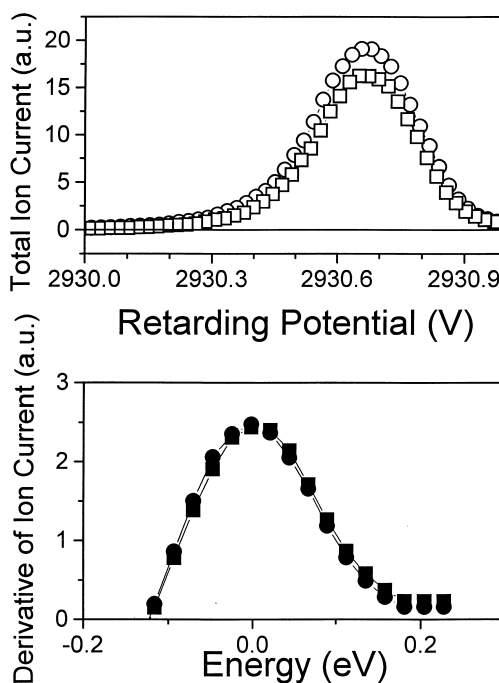


Fig. 4. Upper part: Total reflected ion current measured with the time of flight mass spectrometer in an all-ion mode vs. the retarding potential voltage for  $C_{60}^+$  (designated by open circles) and  $C_{58}^+$  (designated by open squares) primary ions. Lower part: First derivative of the leading edge of the curve shown in the upper part thus yielding the kinetic energy distribution of the respective primary ions (designated by the respective filled symbols) exhibiting a FWHM of about 170 meV in both cases.

surface is defined by the potential difference between the ion source and the surface. The potential difference (hence, the collision energy) can be varied from 0 to about 2 keV with a typical resolution better than about 200 meV. We have determined the energy and a measure for the energy spread of the primary ion beam by using the surface as a retarding potential and measuring the (reflected) total ion signal as a function of the surface potential. Assuming no influence from the detection system on the shape of the retarding potential field ion curve (upper panel in Fig. 4) a measure for the energy spread is given by the full width at half maximum (FWHM) of the first derivative of the total ion signal (lower panel in Fig. 4). Fig. 4 shows as an example in the upper panel the total reflected ion current for the impact of the  $C_{60}^+$  and  $C_{58}^+$

ions, respectively, as a function of the nominal retarding potential in the vicinity of the ion acceleration potential of approximately 2930 V. If the retarding potential is kept above the acceleration potential, no ions will hit the surface and thus no ions will be detected; if the retarding potential is lowered, primary ions will start to be deflected by the surface and the reflected ion current will strongly increase to its peak value. The ensuing decrease of the reflected ion current with decreasing retarding potential (amounting to increasing collision energy) is due to the loss of primary ions at the surface via neutralization processes. The derivative of the leading edge of the total reflected ion currents shown in the lower panel of Fig. 4 indicates in this case a FWHM for the primary ion beam spread of about 170 meV for both ions.

A fraction of the secondary ions formed at the surface exits the shielded chamber through a 1-mm-diameter orifice. These ions are then subjected to the pulsed extraction and acceleration fields, which initiate time-of-flight analysis of these ions. This second mass analyzer is a linear time-of-flight mass selector with a flight tube of about 80 cm in length. The mass selected ions are detected by a double stage multichannel plate which is connected to a fast scaler (with a time resolution of 5 ns per channel) and a laboratory computer. Mass resolution has been improved steadily the past two years and is currently approximately 100. Since it is also possible to pulse the incoming primary ion beam (usually this beam is operated in continuous mode), information on the time dependence of the secondary ion emission and thus on the dynamics of the ion formation processes occurring at the surface can be obtained. Whereas at short delay times the dominant secondary ions are the small secondary fragment ions, at the longer delay times the parent ion group is usually dominating. It is noteworthy that not only the relative abundance of the different secondary ions is changing with delay time, but also the absolute secondary ion current is depending on this parameter. Clearly, one reason for this different behavior of the light and heavy ions could be the occurrence of different velocity distributions (for details on translational energy and velocity distribu-

tions of secondary ion products for surface impact see [40]).

### 3. Results

#### 3.1. Spontaneous decay

For the present study multiply charged carbon cluster ions,  $C_n^{z+}$  ( $n = 36-70$  and  $z = 1-5$ ), are produced by electron impact ionization and dissociation of pure  $C_{70}$  yielding unfragmented parent ions  $C_{70}^{z+}$  and the various fragment ions with  $n < 70$ . Mass spectrometers analyze ions according to their mass-per-charge ratio and therefore, differently charged ions may contribute to the same ion signal. For example, at a mass-per-charge ratio of 180 Thomson the following carbon cluster ions may contribute to the ion signal:  $C_{15}^+$ ,  $C_{30}^{2+}$ ,  $C_{45}^{3+}$ , and  $C_{60}^{4+}$ . As carbon in its natural form consists of two stable isotopes,  $^{12}\text{C}$  (98.89%) and  $^{13}\text{C}$  (1.11%) [41], the ion yield of a carbon cluster with a given size  $n$  will include ions with a well-defined mass distribution pattern which can be calculated using the following simple equation for the relative probability  $p$ :

$$p(^{12}\text{C}_a^{13}\text{C}_b) = \frac{(a+b)!}{a! \cdot b!} \cdot p(^{12}\text{C})^a \cdot p(^{13}\text{C})^b \quad (8)$$

In the case of multiply charged cluster ions, the mass peak containing one  $^{13}\text{C}$  is always located at non-integer mass-per-charge ratios and therefore, in most cases of interest in the present context, free of coincidences (a notable exception however is the coincidence of the ion  $C_{30}^{2+}$  containing one  $^{13}\text{C}$  with the ion  $C_{60}^{4+}$  containing two  $^{13}\text{C}$  isotopes). These peaks can be used for both the identification and the quantitative determination of the ion yield (see [17,26]).

For cluster sizes  $n = 50-70$  and charge states  $z = 1-5$  the total ion yield for ions produced in our Nier-type ion source by the interaction of a  $C_{70}$  beam with a high current electron beam (for details see [7,26]) was determined from these measured isotopic peak patterns. In Fig. 5 the ratio of the ion signal  $C_n^{z+}/C_{70}^{z+}$  is plotted as a function of the cluster size and charge state. The plot clearly shows a strong

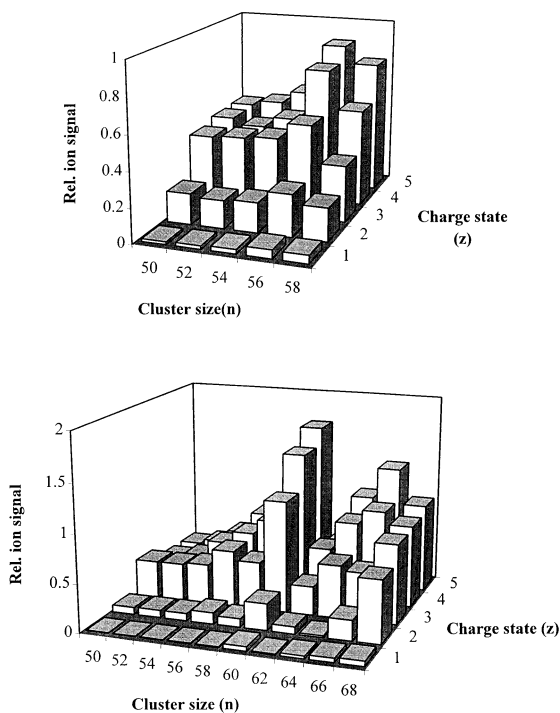


Fig. 5. Normalized fragment ion currents  $C_n^{z+}/C_{60}^{z+}$  and  $C_n^{z+}/C_{70}^{z+}$  for the electron impact ionization of  $C_{60}$  (upper part) and  $C_{70}$  (lower part), respectively.

dependence of this ratio on the charge state (see also measured partial ionization cross sections [33,42] showing a similar tendency). The strong increase for the relative abundance of the fragment ions for higher charge states can be explained most easily by a corresponding strong decrease of the respective  $C_{70}^{z+}$  ion signal. If instead of  $C_{70}$ , pure  $C_{60}$  is ionized in the ion source a similar relative increase of the ion yield for multiply charged fragment ions with increasing charge state (see upper part in Fig. 5) is observed. Thus in both cases for higher charge states the abundance of the unfragmented parent ion is smaller in relation to the fragment ions produced than in the case of singly charged ions.

In a recent article Foltin et al. [27] demonstrated that the reaction probability for the unimolecular evaporation of a  $C_2$  unit from  $C_{60}^{z+}$  via



increases with the charge state when  $z = 1-3$ . In the present article these unimolecular dissociation studies were extended both in the range of the cluster size and the charge state. For a given cluster  $C_n^{z+}$  we have measured the ion yield of all possible fragment ions which are formed by a unimolecular dissociation in the second field-free region. For charge states lower than 3 the only fragmentation process of significance is the evaporation of a neutral  $C_2$  in analogy to reaction (9). The loss of four carbon atoms via



is two orders of magnitude smaller in its intensity and could be identified recently as a sequential  $C_2$  evaporation [27,43]. For higher charge states in addition to  $C_2$  loss also the loss of a  $C_2^+$  and a  $C_4^+$  ion via



was observed [7,25] and taken here into consideration (loss of  $C_6^+$  observed recently [44] is only a minor channel). The Coulomb repulsion in the case of charged particle evaporation reactions (11a) and (11b) (see also below) leads, in contrast in the situation for neutral evaporation reactions (9) and (10), to rather broad MIKE peaks, which even may exhibit a minimum at the center of the peak due to discrimination effects. The height of a measured MIKE peak is certainly not a good measure for the total ion yield of a fragment ion. Here we use the area of the peaks normalized with the sector field value of the center position of the peak. This normalization procedure is necessary because the width of a MIKE peak scales with the sector field value of the center of the peak [44]. The sum of the area of these MIKE peaks is divided by the area of the parent ion  $C_n^{z+}$  peak thus giving a measure for the total metastable fraction.

In Fig. 6 this total metastable fraction is plotted for  $C_{60}^{z+}$  ions (produced in the ion source by electron impact ionization of  $C_{60}$ ) versus the charge state  $z$ . From the increase of this total metastable fraction with increasing charge state it can be concluded that

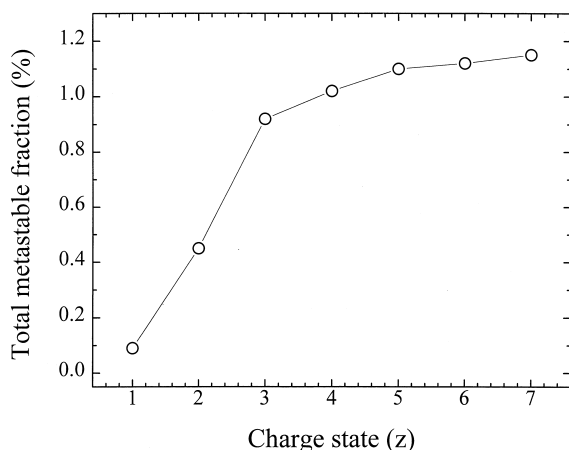


Fig. 6. Total metastable fraction (measured metastable ion current divided by the measured parent ion current, see text) for the decay of  $C_{60}^{z+}$  ions measured via MIKE scans of the various fragment ions in the second field-free region.

the stability of these fullerene parent ions is lowered with increasing charge state. This is in line with the results obtained previously from the mass spectra and shown in Fig. 5. The total metastable fraction was also determined for triply and quadruply charged  $C_n^{z+}$  ions in the size range  $36 \leq n \leq 70$  produced by electron impact ionization of  $C_{70}$  in the ion source. The results are plotted in Fig. 7 as a function of the cluster size. There is a general trend in both charge states that the

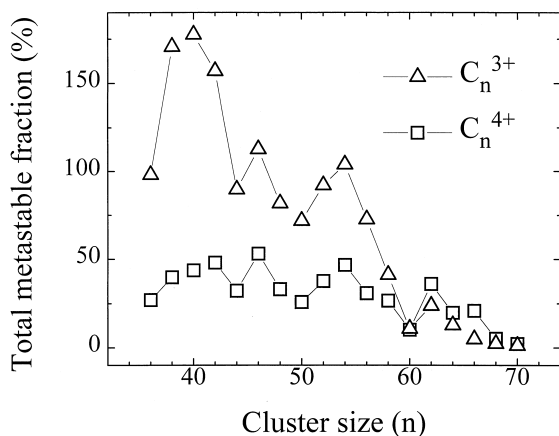


Fig. 7. Total metastable fraction for the decay of triply and quadruply charged carbon cluster ions  $C_n^{z+}$  measured via MIKE scans of the respective fragment ions in the second field-free region.

stability of these fragment ions is smaller with decreasing cluster size. In both data sets the well known magic numbers [45,46]  $n = 60, 50, 44,$  and  $36$  can be clearly seen as local minima in the metastable fraction thus indicating increased relative stability. Surprisingly for smaller fragment ions ( $n < 60$ ) the metastable fraction for the triply charged carbon cluster ions is larger than for quadruply charged fullerenes. This is in contrast to the results shown in Fig. 5, which indicate a decrease in the stability for higher charge states. Nevertheless this tendency is in agreement with observations in direct mass spectra (for ions formed in the ion source) where the minimum of the bimodal distribution which is located at a cluster size of about  $n = 30$  becomes less pronounced in the case of higher charged ions [13,26,47].

Recently, the unimolecular dissociation reaction of highly charged fullerene ions has been investigated and discussed with particular emphasis on reactions leading to charge separation [25,26,28,43,48]. All experimental results indicate that the formation of a charged small fragment ion during the course of such a decay reaction proceeds via an electron transfer from an initially neutral receding fragment to the highly charged fullerene ion (see also [49]). This process has been termed auto-charge-transfer (ACT) and it could be shown in a qualitative manner that with increasing charge state this process becomes the dominant decay reaction as compared to neutral  $C_2$  evaporation. For triply and quadruply charged fullerenes the  $C_2^+$  and  $C_4^+$  evaporation was investigated in detail by the analysis of MIKE scans for cluster sizes  $36 \leq n \leq 70$ . The kinetic energy release and the distance of the fragment ions at the instance of their formation was determined and the results have been discussed elsewhere [28]. Here we want to compare in a more quantitative manner the probability for the occurrence of the two competing decay mechanisms, i.e. neutral and charged fragment loss. This is done by comparing the measured MIKE peaks for the  $C_2^+$  and  $C_4^+$  evaporation to the measured MIKE peaks for the neutral  $C_2$  loss. Thus Fig. 8 shows the ratio of the total fragment ion yield for charged particle loss in comparison to the neutral  $C_2$  evaporation as a function of the charge density ( $z/n$ ) of the parent ion reduced

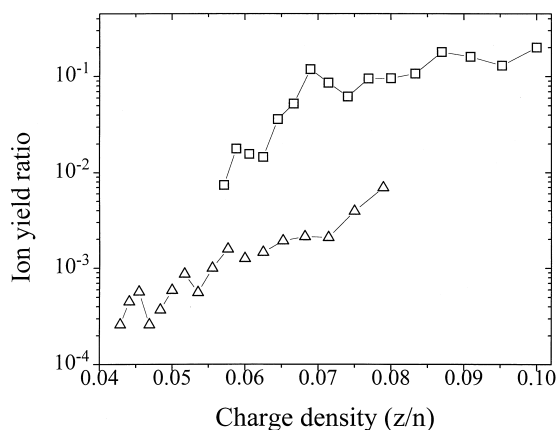


Fig. 8. Ratio of total fragment ion yield for charged particle loss to neutral  $C_2$  evaporation. Symbols as in Fig. 7.

by the mass of the fragment. The ratio is plotted in a logarithmic way and the triangles correspond to triply charged precursor ions whereas the squares are the data points of the quadruply charged ions. For  $C_{60}^{z+}$  ions ( $3 \leq z \leq 7$ ) it was found that the probability for  $C_2^+$  evaporation increases strongly with  $z$  [26]. The charge density  $z/n$  of  $C_{56}^{4+}$  is the same as the charge density of  $C_{42}^{3+}$ . Fig. 8 can give an answer to the question, whether or not the charge density (which is for the case of fullerenes charge per unit area as  $n$  is proportional to the surface area) is determining the ratio of the fragmentation channels ( $C_2^+$  and  $C_2$  loss). Both curves show a similar behavior and the slope in this semilogarithmic plot is almost the same but for the quadruply charged ions the  $C_2^+$  loss is about an order of magnitude more likely than in the case of triply charged fullerenes having the same charge density. This means that the charge density cannot be the parameter responsible for the strong increase of the charge separation decay channel with increasing charge state.

### 3.2. Electron-induced decay

Preliminary measurements of the KERD for the  $C_2$  loss of singly, doubly, triply, and quadruply charged  $C_{58}^{z+}$ ,  $C_{60}^{z+}$ , and  $C_{70}^{z+}$  ions in the second field-free region of our two sector field mass spectrometer

yielded apparent  $\langle KER \rangle$  values increasing strongly with the charge state (see Fig. 5 in [50]). This increase was in contrast to findings by Lifshitz and co-workers [51] who reported  $\langle KER \rangle$  values for  $C_{60}^+$  and  $C_{60}^{2+}$ , which were of about the same value. Moreover, our preliminary  $\langle KER \rangle$  value for  $C_{60}^+$  was larger by about 15% than several values reported by Lifshitz and co-workers [51,52]. In order to resolve this apparent discrepancy we carried out ion trajectory calculations simulating the decay of fullerene ions in our second field-free region as a function of charge state, for different beta slit widths, and for different acceptance angles at the beta slit [35,37]. It turned out that the shape of the calculated KERD is strongly depending on these parameters and that (1) the derived  $\langle KER \rangle$  values deviate from the true values if the beta slit width and the acceptance angle are too large and that (2) this artifact is worsening with increasing charge state of the considered ion. With this in mind we have repeated our earlier measurements with improved experimental conditions (in particular we have decreased the beta slit width from about 2 mm to about 0.2 mm and simultaneously narrowing the mass spectrometer exit slit considerably) thereby being able to reproduce the  $C_{60}^+$  and  $C_{60}^{2+}$  values of Lifshitz and co-worker [53] and to extend the measurements to  $C_{60}^{z+}$  ions with charge states up to  $z = 4$  [35] and to deduce from the measured KERD corresponding activation energies for the neutral loss via reaction (9) [36]. For details see [35,36].

As mentioned in a recent review by Baer and Hase [54] the determination of the KERD for the unimolecular decay of (excited) molecular ions yields valuable information on the energetics and dynamics of the fragmentation reaction. This is even more so if it is possible to measure this property as a function of time after the formation of the excited ion. For instance, a change in  $\langle KER \rangle$  with increasing lifetime of the excited ion may give valuable information on the transition state, i.e. decreasing  $\langle KER \rangle$  with increasing lifetime indicating the absence of a reverse activation barrier [55] and approximately constant  $\langle KER \rangle$  indicating the presence of such a barrier [56].

One way to measure the KERD as a function of ion lifetime is to vary the starting time of the respective

sampling time window, which can be achieved either by changing the accelerating voltage of a two sector field mass spectrometer [57] (for the nominal accelerating voltage of 3 kV used in the present study the time delay between formation of the ion in the ion source and the arrival in the second field-free region is about 50  $\mu$ s) or by varying the delay between the ion formation and the ion extraction in an ion trap/reflectron combination [52,53]. In both cases the KERD is measured for spontaneously decaying ions. Here we use a different approach in that we study the KERD of electron-induced fragmentation of mass selected ions thus giving us the possibility to monitor the decay reaction right after the excitation of the corresponding ion (covering a time window extending from zero up to a few microseconds). Thus, in the case of a decay reaction without reverse barrier (as assumed by several authors for  $C_2$  loss from fullerene ions [58–60]) we expect for these electron-induced decay reactions slightly larger kinetic energies.

Our first measurements (still using the 2 mm beta slit in order to increase the signal intensity) have been carried out here for the simple dissociative excitation reaction of the singly and doubly charged  $C_{60}$  ion



In this case, we cannot distinguish, when using the electron excitation of the mass selected ions, between decay reactions induced by the electron interaction and spontaneous decay reactions leading to the same fragment ion. Nevertheless, as can be seen in Figs. 9 and 10, the fragment ion peaks, which are produced not only by spontaneous decay reactions but also by electron-induced reactions (electron gun on), consistently show a broadening compared to those peaks produced only by spontaneous decay reactions (electron gun off). Thus these peaks clearly indicate the presence of broader KERD and larger  $\langle$ KER $\rangle$  values for fragment ions produced also by electron induced dissociation.

Moreover, in the present study we have also measured the MIKE peaks for reactions where a mass selected precursor ion (for instance  $C_{60}^+$ , see Fig. 2) is

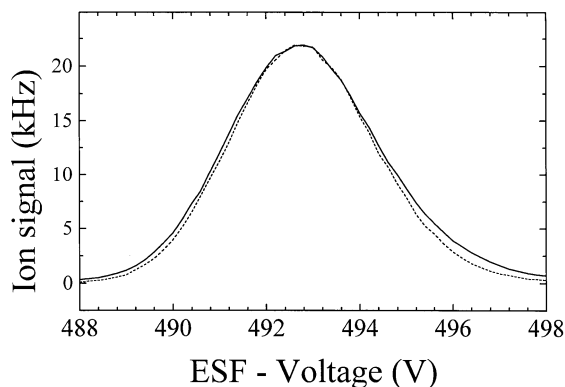


Fig. 9.  $C_{58}^+$  fragment ion peak (MIKE scan) for the spontaneous decay of the  $C_{60}^+$  parent ion (designated by dotted line) and for fragment ions produced by both the spontaneous and electron-induced decay of the parent ion (designated by solid line). Both peaks are normalized to each other at the maximum and recorded with a 2 mm beta slit and wide open mass spectrometer exit slit.

ionized into a higher charge state (for instance  $C_{60}^{2+}$ ) and then the decay of this ionized ion (for instance  $C_{60}^{2+} \rightarrow C_{58}^{2+} + C_2$ ) is analyzed via a MIKE scan of this fragment ion  $C_{58}^{2+}$ . In this case the electron-induced decay reaction is not contaminated by possible spontaneous decay reactions of the mass selected parent ion as in the case of the example given previously [reaction (12a) and (12b)]. Fig. 2 shows MIKE peaks obtained for the following reactions:

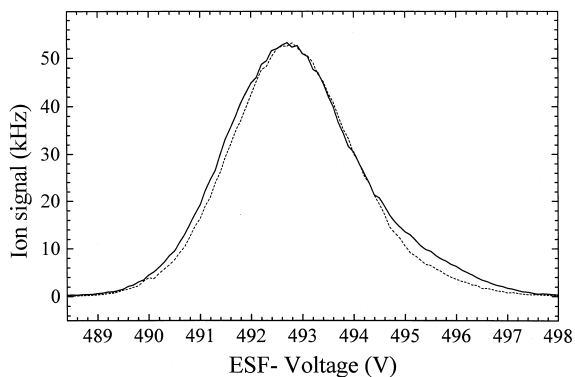


Fig. 10.  $C_{58}^{2+}$  fragment ion peak (MIKE scan) for the spontaneous decay of the  $C_{60}^{2+}$  parent ion (designated by dotted line) and for fragment ions produced by both the spontaneous and electron-induced decay of the parent ion (designated by solid line). Both peaks are normalized to each other at the maximum and recorded with a 2 mm beta slit and wide open mass spectrometer exit slit.



with no coincidence for fragment ions produced by electron-induced decay reactions (13b) and (13c) with possible spontaneous decay reactions of the projectile ion  $\text{C}_{60}^+$ . Therefore, these MIKE peaks can be used directly (i) to determine the kinetic energy release distributions of the fragment ions produced and (ii) to calculate from these KERD the mean kinetic energy release  $\langle \text{KER} \rangle$ . As we have measured these MIKE peaks under experimental conditions (2 mm beta slit and wide open mass spectrometer exit slit) which result in instrumental broadening (see prior discussions and [35,38]) we cannot use the  $\langle \text{KER} \rangle$  values obtained without correcting for this artifact. After proper correction using information gained in our previous study on the KERD for the spontaneous decay of fullerene ions [35,36] we obtain a value of 0.44 eV for the  $\langle \text{KER} \rangle$  of reaction (13b) which is—as expected from theoretical considerations {Rice-Ramsperger-Kassel-Marcus (RRKM) theory [38]}—slightly larger than the corresponding value of 0.41 eV for the spontaneous decay of  $\text{C}_{60}^{2+}$  [35]. In accordance with recent results concerning the singly charged  $\text{C}_{60}^+$  ion by Lifshitz and co-workers using an ion trap reflectron mass spectrometer system [52,53] the presently measured and derived  $\langle \text{KER} \rangle$  values for electron-induced decays of doubly charged fullerene ions (see the comparison shown in Fig. 11) are approximately 10% higher than those for spontaneous decay reactions measured under the same experimental conditions. This strong time dependence is a further confirmation that the reaction (12) does not proceed via a reverse activation barrier in accordance with earlier conjectures [58–60].

### 3.3. Surface-induced processes

Recently, we have measured in a collaboration with the group of Winter and co-workers [61–63] absolute total electron emission yields for impact of carbon cluster ions  $\text{C}_n^{z+}$  on atomically clean gold as a

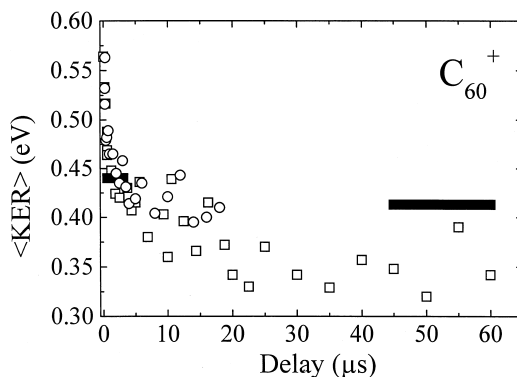


Fig. 11. Average total kinetic energy release  $\langle \text{KER} \rangle$  for the  $\text{C}_2$  loss from  $\text{C}_{60}^+$  as a function of delay time between production of the  $\text{C}_{60}^+$  ion and the decay as measured by Laskin et al. (designated by open squares [52] and open circles [53]). Also shown are the present results for the spontaneous  $\text{C}_2$  loss decay of  $\text{C}_{60}^{2+}$  (designated solid bar at around  $50 \mu\text{s}$ ) and the electron induced decay reaction (13b)  $\text{C}_{60}^+ + e \rightarrow \text{C}_{58}^{2+}$  (designated solid bar around  $2 \mu\text{s}$ ).

function of cluster size (up to  $n = 60$ ), charge (up to  $z = 5$ ) and kinetic energy (up to 165 keV). Besides finding a linear dependence on cluster size  $n$  and an electron emission well below the classical kinetic emission threshold, the overriding conclusion from these experiments is the complete suppression of potential electron emission, i.e. the electron emission yield is independent of the charge state of the projectile ion (a fact which is in contrast to what is known for multicharged atomic ions). Preliminary molecular dynamics calculations [64] suggested that this surprising result may—at least in part—be due to the special nature of potential energy release, which has been proposed to cause enhanced fragmentation rather than electron emission. Thus, in following up these electron emission studies we have therefore recently investigated with the tandem mass spectrometer BESTOF the reactive interaction of multiply charged fullerene ions  $\text{C}_{60}^{z+}$  ( $1 \leq z \leq 5$ ) with various surfaces, including hydrocarbon covered stainless steel and gold surfaces thereby extending the previous measurements of Kappes and co-workers [31,32] for singly charged fullerene ions to multiply charged fullerene ions [65,66]. Besides elastic scattering we have in these recent investigations observed and studied as a function of collision energy surface-

induced dissociation and pick-up reactions. The results for singly charged parent ions are in good agreement with the previous study of Kappes and co-workers [31,32]. Moreover, the strong dependence observed for the two inelastic reaction channels on charge state [65,66], in particular the observed increase in the fragmentation yield with larger charge states supports the suggested explanation given in [63,64] for the suppressed potential electron emission, i.e. that the large potential energy release upon partial or total neutralization (decrease of charge state) of the highly charged fullerene ion upon surface impact is not available for potential emission due to rapid conversion of this electronic energy into vibrational degrees of freedom followed by unimolecular fragmentation of the “reflected” (singly charged) fullerene ion.

Here, we have extended these investigations on surface-induced reactions to the interaction of fullerene ions with sizes below  $n = 60$ , in particular to  $C_{58}^+$  and  $C_{58}^{2+}$  both produced in the ion source as fragment ions via electron impact ionization of a neutral  $C_{60}$  beam. Due to the different formation mechanism of these “fragment” projectile ions  $C_{58}^+$  and  $C_{58}^{2+}$  (as compared to “parent” projectile ions) they will have on average a much larger internal energy [67] before the surface impact than the corresponding parent ions  $C_{60}^+$  or  $C_{60}^{2+}$ . Moreover, the parent ions have a broad internal energy distribution, whereas the energy distribution of the fragment ions is narrow, because only the highest excited parent ions lead to the production of the fragment ions in the ion source. Fig. 12 shows as an example secondary mass spectra obtained for the  $C_{58}^{2+}$  projectile ion for collision energies between 100 and 500 eV. As in the case of  $C_{60}^{2+}$  projectile ions (see [65]) surface induced interaction of  $C_{58}^{2+}$  projectile ions leads—besides to fragmentation—also to appreciable amounts of pick-up reactions, both type of surface induced reactions strongly increasing with collision energy. Nevertheless, there exist several noteworthy differences between the observed reaction behavior for parent projectile ions [65,66] and fragment projectile ions.

It is interesting to note that, in contrast to  $C_{60}^{2+}$  (see [65]) where dissociation reactions are only present for

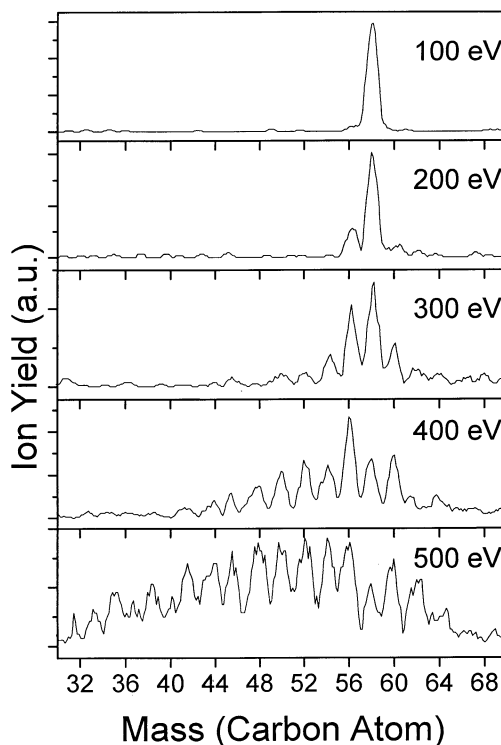


Fig. 12. Product ion mass spectra for the surface impact of  $C_{58}^{2+}$  ions with various collision energies.

energies above about 150 eV, dissociation reactions for  $C_{58}^{2+}$  start to proceed already at energies of around and below 100 eV (see the partial and total reduced product ion yields given as function of the collision energy in Figs. 13 and 14). This lowering of the reaction threshold for the fragment projectile ion can be ascribed to the higher internal energy content of these ions as mentioned above. In this case the activation energy necessary to drive the dissociation reaction is not only provided by collision energy converted to internal energy (according to [32], approximately 15%) but also by the internal energy already present before the surface collision.

Besides this different threshold behavior also the relative shape of the energy dependence and its absolute value is different. As can be seen in Fig. 13 there is no dependence on the charge state in the case of fragment projectile ions for all cases considered, i.e.  $C_2$  loss and  $C_2$  pick-up (middle panel) and  $C_4$  loss

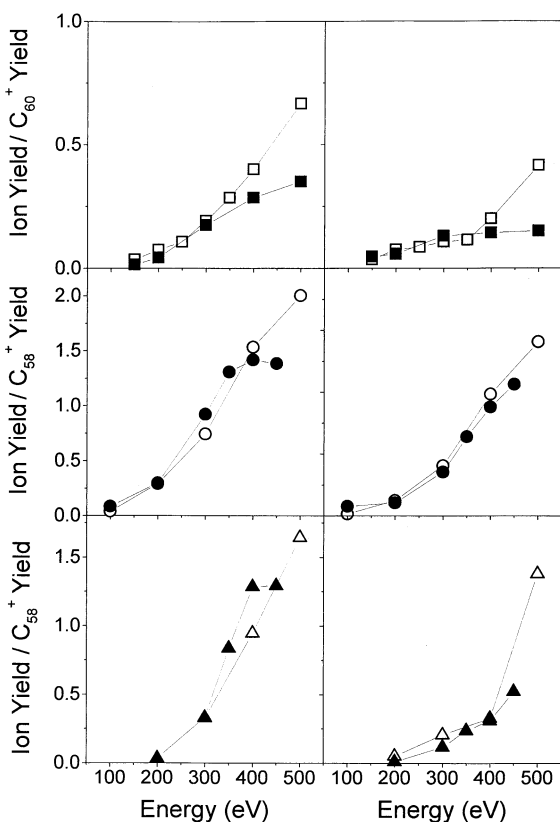


Fig. 13. Normalized product ion yield as a function of collision energy for dissociation reactions (left-hand side) and pick-up reactions (right-hand side) for singly charged (filled symbols) and doubly charged (open symbols) projectile ions. Top panel:  $C_2$  loss and pick-up by  $C_{60}^{z+}$ , middle panel:  $C_2$  loss and  $C_2$  pick-up by  $C_{58}^{z+}$ , bottom panel:  $C_4$  loss and  $C_4$  pick-up by  $C_{58}^{z+}$ .

and  $C_4$  pick-up (bottom panel), whereas for the  $C_{60}^{z+}$  ions the relative ion yield for both loss and pick-up reactions (top panel) increases for doubly charged ions stronger with collision energy than for singly charged ions. A similar tendency can be seen in Fig. 14 for the total relative secondary ion yield. It is conceivable that this tendency (a strong dependence on charge state of the product ion yield for parent projectile ions [65,66] and a much lesser dependence on the charge state for the  $C_{58}^{z+}$  projectile ions C as demonstrated in more detail in Figs. 15 and 16) is caused by the different internal energy content of these two types of projectile ions. In addition, the

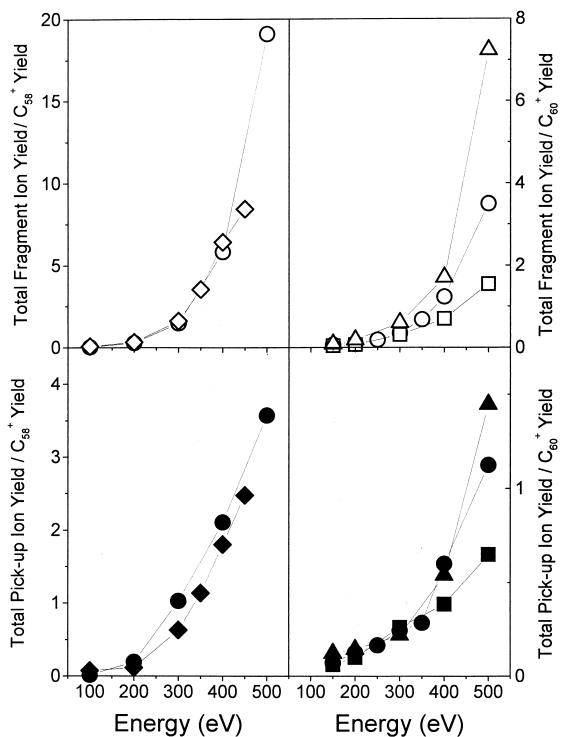


Fig. 14. Normalized product ion yield vs. collision energy for dissociation reactions (open symbols) and pick-up reactions (filled symbols). Singly charged  $C_{58}^{z+}$  and  $C_{60}^{z+}$  ions: diamonds and squares, doubly charged  $C_{58}^{2+}$  and  $C_{60}^{2+}$  ions: circles, and triply charged  $C_{60}^{3+}$  ions: triangles.

absolute yields in Figs. 13 and 14 are in the energy range probed by approximately a factor of 2 larger for the fragment projectile ions as compared to the parent projectile ions. This latter observation may again be ascribed to the higher internal energy content prior to surface interaction of the fragment projectile ions in comparison to the parent projectile ions.

## Acknowledgements

This work was supported in part by the FWF, the ÖNB, and the BMWV, Wien, Austria. One of the authors (P.S.) would like to thank the Austrian Academy of Sciences, Wien, for support through an APART grant.

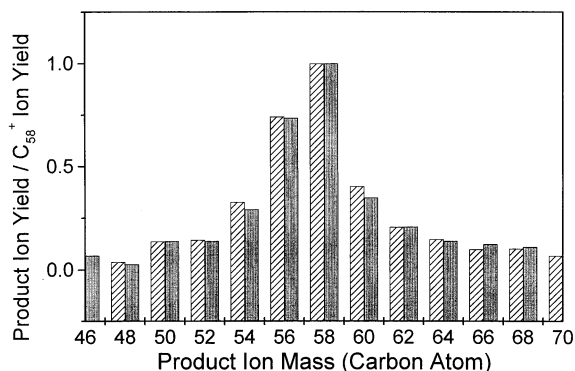


Fig. 15. Normalized product ion yield for singly charged (shaded bars) and doubly charged (hatched bars)  $C_{58}^{+}$  projectile ions vs. product ion mass at 300 eV collision energy.

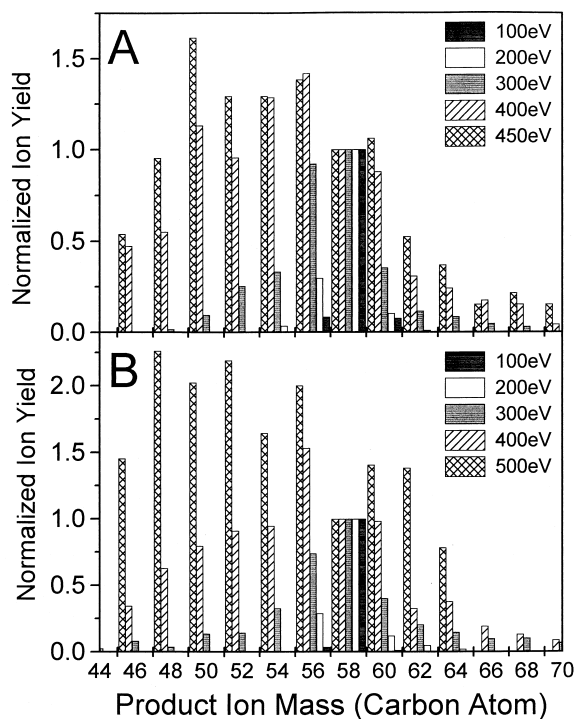


Fig. 16. Normalized product ion yield for singly charged (upper panel) and doubly charged (lower panel)  $C_{58}^{+}$  projectile ions vs. product ion mass at different collision energies. Note that the highest collision energy for which data are shown in the two panels is different.

## References

- [1] O. Echt, T.D. Märk, in *Clusters of Atoms and Molecules*, H. Haberland (Ed.), Springer, Heidelberg, 1994, Vol. II, p. 183.
- [2] H.W. Kroto, J.R. Heath, S.C. O'Brien, R.F. Curl, R.E. Smalley, *Nature* 318 (1985) 162.
- [3] C.W. Walter, Y.K. Bae, D.C. Lorents, J.R. Peterson, *Chem. Phys. Lett.* 195 (1992) 543.
- [4] S. Petrie, J. Wang, D.K. Bohme, *Chem. Phys. Lett.* 204 (1993) 473.
- [5] P. Scheier, R. Robl, B. Schiestl, T.D. Märk, *Chem. Phys. Lett.* 220 (1994) 141.
- [6] P. Scheier, T.D. Märk, *Int. J. Mass Spectrom. Ion Processes* 133 (1994) L5.
- [7] P. Scheier, T.D. Märk, *Phys. Rev. Lett.* 73 (1994) 54.
- [8] J. Jin, H. Khemliche, M.H. Prior, Z. Xie, *Phys. Rev. A* 53 (1996) 615.
- [9] J. Cioslowski, S. Patchovskii, W. Thiel, *Chem. Phys. Lett.* 248 (1996) 116.
- [10] G. Seifert, R. Gutierrez, R. Schmidt, *Phys. Lett. A* 211 (1996) 357.
- [11] J. Opitz, S. Jacquet, U. Werner, H.O. Lutz, B. Huber, *Proceedings of the 17th International Symposium on Molecular Beams*, Orsay, 1997, p. 131.
- [12] C.E. Klots, *Z. Phys. D* 21 (1991) 335.
- [13] S.W. McElvany, M.M. Ross, J.H. Callahan, *Acc. Chem. Res.* 25 (1992) 162.
- [14] C. Lifshitz, *Mass Spectrom. Rev.* 12 (1993) 261.
- [15] H. Schwarz, *Nova Acta Leopoldina* 69 (1993) 167.
- [16] E. Kolodney, B. Tsipinyuk, A. Budrevich, *J. Chem. Phys.* 102 (1995) 9263.
- [17] P. Scheier, B. Dünser, R. Wörgötter, S. Matt, D. Muigg, G. Senn, T.D. Märk, *Int. Rev. Phys. Chem.* 15 (1996) 93.
- [18] K. Hansen, E.E.B. Campbell, *J. Chem. Phys.* 104 (1996) 5012.
- [19] R. Hippler, M. Quack, R. Schwarz, G. Seyfang, S. Matt, T.D. Märk, *Chem. Phys. Lett.* 278 (1997) 111.
- [20] S. Matt, O. Echt, R. Wörgötter, P. Scheier, C.E. Klots, T.D. Märk, *Int. J. Mass Spectrom. Ion Processes* 167/168 (1997) 753.
- [21] S. Matt, P. Scheier, T.D. Märk, K. Becker, in *Novel Aspects of Electron–Molecule Collisions*, K. Becker (Ed.), World Scientific, Singapore, 1998, pp. 1–56.
- [22] J. Laskin, B. Hadas, T.D. Märk, C. Lifshitz, *Int. J. Mass Spectrom.* 177 (1998) L9.
- [23] A.D. Boese, G.E. Scuseria, *Chem. Phys. Lett.* 294 (1998) 233.
- [24] S.W. McElvany, M.M. Ross, D.K. Bohme (Eds.), *Special issue on fullerenes, carbon, and metal–carbon clusters*, *Int. J. Mass Spectrom. Ion Processes* 138 (1994).
- [25] P. Scheier, B. Dünser, T.D. Märk, *Phys. Rev. Lett.* 74 (1995) 3368.
- [26] P. Scheier, B. Dünser, T.D. Märk, *J. Phys. Chem.* 99 (1995) 15437.
- [27] M. Foltin, O. Echt, P. Scheier, B. Dünser, R. Wörgötter, D. Muigg, S. Matt, T.D. Märk, *J. Chem. Phys.* 107 (1997) 6246.
- [28] G. Senn, T.D. Märk, P. Scheier, *J. Chem. Phys.* 108 (1998) 990.
- [29] R. Völpel, G. Hofmann, M. Steidl, M. Stenke, M. Schlapp, R. Trassl, E. Salzborn, *Phys. Rev. Lett.* 71 (1993) 3439.
- [30] T. Rauth, O. Echt, P. Scheier, T.D. Märk, *Chem. Phys. Lett.* 247 (1995) 515.

- [31] P. Weis, J. Rockenberger, R.D. Beck, M.M. Kappes, *J. Chem. Phys.* 104 (1996) 3629.
- [32] R.D. Beck, J. Rockenberger, P. Weis, M.M. Kappes, *J. Chem. Phys.* 104 (1996) 3638.
- [33] S. Matt, B. Dünser, M. Lezius, H. Deutsch, K. Becker, A. Stamatovic, P. Scheier, T.D. Märk, *J. Chem. Phys.* 105 (1996) 1880.
- [34] R.G. Cooks, J.H. Beynon, R.M. Caprioli, G.R. Lester, *Metastable Ions*, Elsevier, Amsterdam, 1973.
- [35] S. Matt, M. Sonderegger, R. David, O. Echt, P. Scheier, J. Laskin, C. Lifshitz, T.D. Märk, *Int. J. Mass Spectrom.* 185/186/187 (1999) 813.
- [36] S. Matt, O. Echt, M. Sonderegger, R. David, P. Scheier, J. Laskin, C. Lifshitz, T.D. Märk, *Chem. Phys. Lett.* 303 (1999) 379.
- [37] S. Matt, M. Sonderegger, R. David, T. Fiegele, C. Mair, F. Biasioli, A. Stamatovic, P. Scheier, T.D. Märk, in *Elementary Processes and Chemical Reactions in Low Temperature Plasmas*, M. Morvava, K. Hensel (Eds.), Bratislava University, 1998, ISBN No. 80 967454-6-8, pp. 136–156.
- [38] S. Matt, Ph.D. Thesis, Universität Innsbruck, 1998.
- [39] C. Mair, T. Fiegele, F. Biasioli, R. Wörgötter, V. Grill, M. Lezius, T.D. Märk, *Plasma Sources Sci. Technol.* 8 (1999) 1.
- [40] R. Wörgötter, J. Kubista, J. Zabka, Z. Dolejssek, T.D. Märk, Z. Herman, *Int. J. Mass Spectrom. Ion Processes* 177 (1998) 105.
- [41] *CRC Handbook of Chemistry and Physics*, D.R. Lide (Ed.), CRC, Boca Raton, FL, 1990, pp. 11–34.
- [42] V. Foltin, M. Foltin, S. Matt, P. Scheier, K. Becker, H. Deutsch, T.D. Märk, *Chem. Phys. Lett.* 289 (1998) 181.
- [43] P. Scheier, B. Dünser, D. Muigg, S. Matt, O. Echt, M. Foltin, T.D. Märk, *Phys. Rev. Lett.* 77 (1996) 2654.
- [44] G. Senn, B. Dünser, P. Scheier, T.D. Märk, *Chem. Phys. Lett.* 266 (1997) 276.
- [45] S.C. O'Brian, J.R. Heath, R.F. Curl, R.E. Smalley, *J. Chem. Phys.* 88 (1988) 220.
- [46] P.P. Radi, M.T. Hsu, J. Brodtbelt-Lustig, M. Rincon, M.T. Bowers, *J. Chem. Phys.* 92 (1990) 4817.
- [47] S. Matt, P. Scheier, A. Stamatovic, H. Deutsch, K. Becker, T.D. Märk, *R. Soc. London, Ser. A*, in press.
- [48] B. Dünser, O. Echt, P. Scheier, T.D. Märk, *Phys. Rev. Lett.* 79 (1997) 3861; P. Scheier, G. Senn, S. Matt, T.D. Märk, *Int. J. Mass Spectrom. Ion Processes* 172 (1998) L1.
- [49] P.M. Gill, L. Radom, *J. Am. Chem. Soc.* 110 (1988) 5311.
- [50] S. Matt, A. Stamatovic, M. Sonderegger, P. Scheier, T. Märk, *Book of Abstracts, 17th International Symposium on Molecular Beams*, Orsay, 1997, p. 263.
- [51] C. Lifshitz, M. Iraqi, T. Peres, J.E. Fischer, *Int. J. Mass Spectrom. Ion Processes* 107 (1991) 565.
- [52] J. Laskin, C. Weikhardt, C. Lifshitz, *Chem. Phys. Lett.* 161 (1997) L7.
- [53] J. Laskin, C. Lifshitz, *Isr. J. Chem.* 37 (1997) 467.
- [54] T. Baer, W.L. Hase, *Unimolecular Reaction Dynamics, Theory and Experiments*, Oxford University Press, New York, 1996.
- [55] C. Lifshitz, P. Gotchiguian, R. Roller, *Chem. Phys. Lett.* 95 (1984) 106.
- [56] C. Lifshitz, S. Gefen, R. Arakawa, *J. Phys. Chem.* 88 (1984) 4242.
- [57] Y. Ji, M. Foltin, C.H. Liao, T.D. Märk, *J. Chem. Phys.* 96 (1992) 3624.
- [58] P.P. Radi, M.T. Hsu, M.E. Rincon, P.R. Kemper, M.T. Bowers, *Chem. Phys. Lett.* 174 (1991) 335.
- [59] P. Sandler, C. Lifshitz, C.E. Klots, *Chem. Phys. Lett.* 200 (1992) 445.
- [60] J. Laskin, H.A. Jimenez-Vazquez, R. Shimshi, M. Saunders, M.S. deVries, and C. Lifshitz, *Chem. Phys. Lett.* 242 (1995) 249.
- [61] K. Tögelhofer, F. Aumayr, H. Kurz, HP. Winter, P. Scheier, T.D. Märk, *J. Chem. Phys.* 99 (1993) 8254.
- [62] F. Aumayr, M. Vana, HP. Winter, H. Drexel, V. Grill, G. Senn, S. Matt, P. Scheier, T.D. Märk, *Int. J. Mass Spectrom. Ion Processes* 163 (1997) L9.
- [63] HP. Winter, M. Vana, G. Betz, F. Aumayr, H. Drexel, P. Scheier, T.D. Märk, *Phys. Rev. A* 56 (1997) 3007.
- [64] F. Aumayr, G. Betz, T.D. Märk, P. Scheier, HP. Winter, *Int. J. Mass Spectrom. Ion Processes* 174 (1998) 317.
- [65] T. Fiegele, F. Biasioli, C. Mair, T.D. Märk, F. Aumayr, G. Betz, HP. Winter, *Book of Abstract, ERC Symposium on Cluster Surface Interaction*, S. Matt, T.D. Märk, K.H. Meiwes-Broer (Eds.), Cargese, 1998, p. 63.
- [66] F. Biasioli, T. Fiegele, C. Mair, F. Aumayr, G. Betz, HP. Winter, T.D. Märk, unpublished.
- [67] M. Foltin, M. Lezius, P. Scheier, T.D. Märk, *J. Chem. Phys.* 98 (1993) 9624.